ACS OMEGA

http://pubs.acs.org/journal/acsodf

Article

Reactions of Methyl Radicals with Aniline Acting as Hydrogen Donors and as Methyl Radical Acceptors

Tien V. Pham* and Hoang T. T. Trang*

Cite This: *ACS Omega* 2023, 8, 17005−17016

Read Online

ACCESS | Metrics & More | Article Recommendations | Supporting Information

ABSTRACT: The present investigation theoretically reports the comprehensive kinetic mechanism of the reaction between aniline and the methyl radical over a wide range of temperatures (300−2000 K) and pressures (76−76,000 Torr). The potential energy surface of the $C_6H_5NH_2$ + CH_3 reaction has been established at the CCSD(T)//M06-2X/6-311++G(3df,2p) level of theory. The conventional transition-state theory (TST) was utilized to calculate rate constants for the elementary reaction channels, while the stochastic RRKM-based master equation framework was applied for the *T*- and *P*-dependent rate-coefficient calculation of multiwell reaction paths. Hindered internal rotation and Eckart tunneling treatments were included. The H-abstraction from the $-NH_2$ group of aniline (to form P1 (C_6H_5NH + CH_4)) has been found to compete with the CH_3-addition on the C atom at the ortho site of aniline (to form IS2) with the atmospheric rate expressions (in cm^3 molecule^{-1} s^{-1}) as $k_{a1} = 7.5 \times 10^{-23}\ T^{3.04} \exp[(-40.63 \pm 0.29\ \text{kJ·mol}^{-1})/RT]$ and $k_{b2} = 2.29 \times 10^{-3}\ T^{-3.19} \exp[(-56.94 \pm 1.17\ \text{kJ·mol}^{-1})/RT]$ for T = 300−2000 K and P = 760 Torr. Even though rate constants of several reaction channels decrease with increasing pressures, the total rate constant $k_{total} = 7.71 \times 10^{-17}\ T^{1.20} \exp[(-40.96 \pm 2.18\ \text{kJ·mol}^{-1})/RT]$ of the title reaction still increases as the pressure increases in the range of 76−76,000 Torr. The calculated enthalpy changes for some species are in good agreement with the available experimental data within their uncertainties (the maximum deviation between theory and experiment is ∼11 kJ·mol^{-1}). The T1 diagnostic and spin contamination analysis for all species involved have also been observed. This work provides sound quality rate coefficients for the title reaction, which will be valuable for the development of detailed combustion reaction mechanisms for hydrocarbon fuels.

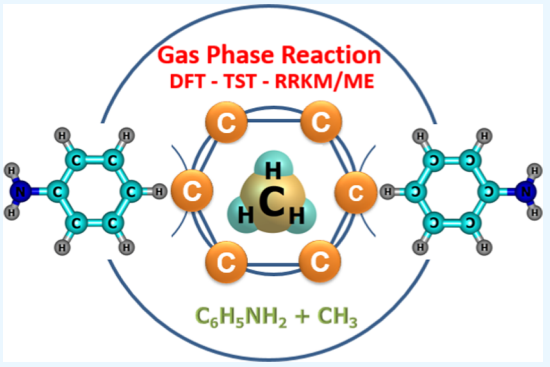

1. INTRODUCTION

Aniline ($C_6H_5NH_2$), consisting of a benzene ring attached to an amino group, is the simplest primary aromatic amine. It is an important precursor to manufacture a wide range of products used in our daily life, including polyurethane foam, agricultural chemicals, synthetic dyes, antioxidants, paints, fabrics, rubbers, herbicides, varnishes, drugs, and explosives. It is worth mentioning that many industrial processes, encompassing both the manufacture and application of aniline, have substantially contributed to the rise in atmospheric aniline emissions. These emissions have reached concentrations of up to tens of parts per trillion by volume (pptv).[1] In the atmosphere, aniline possesses the characteristic of aromatic compounds and ignites immediately with a smoky flame.[2] Aniline and its derivatives can react with atmospheric oxidants and contribute to the formation of secondary organic aerosols (SOAs). In addition, it is considered a hazardous air pollutant (HAP) and has been listed by the United States Environmental Protection Agency (EPA) as a priority pollutant due to its toxicity and potential risks to human health and the environment.[3,4] Some kinds of common diseases (e.g., anemia, headaches, tremor, paresthesia, pain, narcosis or coma, cardiac arrhythmia, and heart, kidney, and liver damage) occurring in humans are thought to be related to aniline if people are regularly exposed to this substance.[5] Oxidation of amine compounds including aniline often leads to N-centered radicals, which can highly react with atmospheric gases such as nitrogen monoxide and nitrogen dioxide instead of reacting with oxygen molecules to form carcinogenic nitrosamines and nitramines[6−12] because the reaction between N-centered radicals and oxygen molecules often occurs slowly; thus, these radicals when formed should possibly be removed by atmospheric species.[12,13]

Another moiety of the reactants, methyl radical (CH_3) known as an isoelectronic species, occurs naturally in the troposphere with very low concentration, typically on the order of 1−10 pptv in clean air; however, it can be much higher in areas with high levels of pollution. This radical is recorded to be a short-lived

Received: February 15, 2023
Accepted: April 19, 2023
Published: May 1, 2023

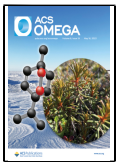

species in the atmosphere with a lifetime on the order of seconds to minutes.[14] Methyl radical is primarily produced in the atmosphere through the photolysis of volatile organic compounds (VOCs) such as methane (CH_4), which is the largest natural source of methyl radical. Anthropogenic sources of VOCs, such as industrial processes and transportation regarding the burning of fossil fuels or biomass, also contribute to the production of methyl radicals in the atmosphere.[15] Furthermore, natural sources such as plant emissions, wetland soils, and oceans can lead to the release of CH_4 or other hydrocarbons into the atmosphere, which can then break down and release CH_3 radicals in the troposphere.[16] Once formed, methyl radical can react with a variety of atmospheric species including oxygen (O_2), nitrogen oxide (NO), and ozone (O_3). Some of the main reactions involving a methyl radical in the troposphere include $CH_3 + O_2 \rightarrow CH_3O_2$ (methyl peroxy radical),[17] $CH_3 + NO \rightarrow HCN + H_2O$,[18] $CH_3 + HO_2 \rightarrow$ products,[19] and $CH_3 + O_3 \rightarrow$ products (ozone depletion reaction).[20] These reactions can have important impacts on atmospheric chemistry, affecting the levels of important pollutants such as ozone, as well as the oxidation capacity of the atmosphere. In addition, the methyl radical not only acts as an important agent in fossil fuel combustion but also plays a key role in the high-temperature oxidation of hydrocarbons.[21] It is considered one of the troposphere's detergents, which is relevant to the removal process of various volatile organic compounds. Therefore, it can react with almost all air pollutants, including the aniline compound.[22,23] Furthermore, it is known that the majority of organic compounds discharged into the atmosphere undergo degradation by reactions with free radicals OH, CH_3, and NO_3 through photolysis and physical mechanisms such as wet and dry deposition.[24] Hence, an accurate understanding of the mechanism and kinetics of the reaction between aniline and the methyl radical is imperative for comprehending the conversion of aniline into other chemical species by CH_3 radicals in the troposphere.

To the best of our knowledge, the mechanism and kinetics of the reaction between $C_6H_5NH_2$ and CH_3 radical, at various temperatures and pressures, have not yet been investigated in both theoretical and experimental aspects, even though the concentrations of aniline and the methyl radical in the atmosphere are relatively high in regions where pollution is particularly severe. It was found that the chemistry of aniline is a prototype for complex nitrogen-containing compounds of potential relevance to combustion applications.[25] Due to the lack of such qualitative and quantitative data, the present study focuses on studying the possibility of explaining the behavior of aniline through the application of quantum mechanical methods. It is anticipated that modern technology may bring a deeper understanding of the associated chemical mechanisms and open the route for further studies of other aromatic amines. Therefore, in the present work, the CCSD(T)//M06-2X/6-311++G(3df,2p) level of theory has been used to thoroughly characterize the potential energy surface (PES) of the $C_6H_5NH_2 + CH_3$ reaction. This reaction was not suggested earlier as a possible source of polycyclic aromatic hydrocarbon precursors, but it is an appropriate representative of the layer of reactions of aromatic molecules with species having a single electron. The mechanism of the $C_6H_5NH_2 + CH_3$ reaction indicates that the reaction can proceed via addition and/or abstraction channels, and the most favorable path can lead to an intermediate, namely, 2-methyl-aniline ($CH_3-C_6H_5NH_2$) or a bimolecular product containing C_6H_5NH and CH_4.

2. COMPUTATIONAL METHODS

In the present study, in order to optimize geometric structures of all species in the $C_6H_5NH_2 + CH_3$ reaction system, we have utilized the density functional theory DFT/M06-2X[26−28] in conjunction with the 6-311++G(3df,2p)[29] basis sets. Vibrational frequencies, moments of inertia, and zero-point vibrational energies (ZPVE) were obtained after optimizing the species involved. The geometries optimized at the M06-2X/6-311++G(3df,2p) level were then employed for the single-point energy calculations at the CCSD(T)/6-311++G(3df,2p)[30] level of theory. The potential energy surface of the $C_6H_5NH_2 + CH_3$ reaction system has been established based on the relative energies of the species computed at the CCSD(T)//M06-2X/6-311++G(3df,2p) + ZPVE level in which the ZPVE values were corrected by a factor of 0.971.[31] This correction was also applied to many previous studies.[32−37] The calculated vibrational frequencies of each species were used to confirm the difference between an intermediate state and a transition state (a saddle point). Normally, all frequencies of a local minimum are positive and a transition state must contain one negative frequency (imaginary frequency). The intrinsic reaction coordinate (IRC)[38,39] was utilized to determine the connection between a transition state (TS) and two stationary points that lie just before and after this TS. All of the calculations in this study were conducted by the Gaussian 16 software package.[40]

Rate constants of the energetically low-lying reaction paths on the PES have been calculated by using the MESMER program[41] whose code was written based on the fundamental theory of kinetics including TST,[42] VRC-TST,[43,44] and RRKM theory[45] with Eckart tunneling corrections.[46] Such a model has been successfully utilized for various gas-phase reaction systems;[47−51] e.g., $C_3H_3 + NH_3$,[47] $C_3H_3 + CH_3$,[49] and $C_2H_3 + C_2H_3$.[50] The sum of state and the density of state were computed with the support of energy barriers, vibrational frequencies, and rotational constants. The master equation[52] involving multistep vibrational energy transfer for the $C_7H_8NH_2$ excited intermediate state was solved to obtain the pressure- and temperature-dependent rate constants using the energy-dependent microcanonical RRKM statistical rate constants, $k(E)$. In this study, the values of Lennard-Jones (L-J) of the bath gas Ar (ε/k_B = 113.50 K, σ = 3.465 Å) and the L-J values of the $C_7H_8NH_2$ intermediate (σ = 5.923 Å, ε = 407.8 K) have been taken from the references.[53,54] The average energy transferred per collision, $\langle \Delta E_{down} \rangle$ = 400 cm^{-1}, was used for the standard form of the "exponential down" model.[55] The suitability of this value for several reaction systems, including $C_6H_5 + NH_2$,[35] $C_3H_3 + NH_3$,[47] and $C_3H_3 + HNCO$,[56] has been discovered. Additionally, the impact of different $\langle \Delta E_{down} \rangle$ values on the outcomes of the $C_6H_5NH_2 + CH_3$ system has been meticulously investigated and deemed insignificant. This serves as the basis for us to utilize it in the current system. The thermochemical properties including enthalpy change (ΔH°_{298K}), Gibbs free energy (ΔG°_{298K}), and entropy change (ΔS°_{298K}) of the system have also been taken into account in comparison with the available literature data to determine the validity of the method used in this calculation.

3. RESULTS AND DISCUSSION

3.1. Potential Energy Surface and Reaction Mechanism. The PES containing the favorable channels of the $C_6H_5NH_2 + CH_3$ reaction system characterized at the CCSD(T)//M06-2X/6-311++G(3df,2p) level of theory is

https://doi.org/10.1021/acsomega.3c01029
ACS Omega 2023, 8, 17005−17016

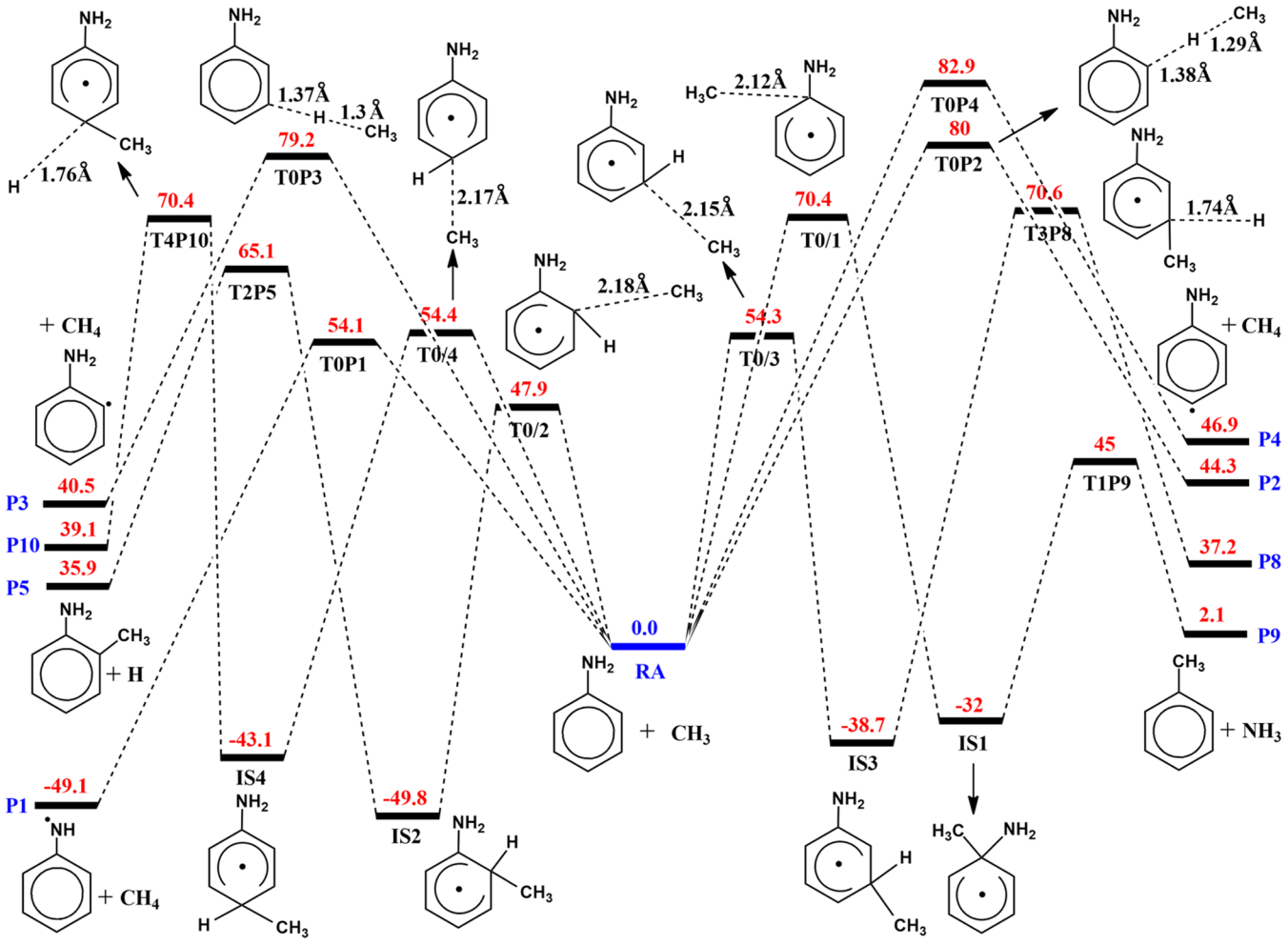

Figure 1. Potential energy surface containing the favorable channels of the $C_6H_5NH_2 + CH_3$ reaction system calculated at the CCSD(T)//M06-2X/6-311++G(3df,2p) + ZPVE level of theory (energies are in kJ·mol^{-1}).

shown in Figure 1 of this work, while the PES holding the unfavorable channels is displayed in Figure S1. The M06-2X/6-311++G(3df,2p) optimized geometries of all species involved are displayed in Figures S2 and S3. Single-point energies and zero-point vibrational energies (ZPVE) for all species predicted at the various levels are presented in Table S1. Heats of formation and heats of reaction (ΔH°_{298K}) in the $C_7H_{10}N$ system were calculated and compared with the experimental data as listed in Table 1. Vibrational frequencies and the complete list of Cartesian coordinates for all substances in the system are tabulated in Tables S2 and S3, respectively, whereas Gibbs free energies (ΔG°_{298K}) and entropies (ΔS°_{298K}) of all channels are presented in Table S4.

It is not difficult to realize that the reaction between the aniline compound and the methyl radical can lead to various bimolecular products, in which the P1−P4 products contain the same species CH_4, the P5, P7, P8, and P10 products contain hydrogen atom, two products (P6, P9) have NH_2 radical, and four products (P11−P13) own the same NH_3 molecule. In detail, the four CH_4-containing products, namely, P1 ($C_6H_5NH + CH_4$), P2 (o-$C_6H_4NH_2 + CH_4$), P3 (m-$C_6H_4NH_2 + CH_4$), and P4 (p-$C_6H_4NH_2 + CH_4$), were produced through the H-abstraction procedures at the saddle points T0P1, T0P2, T0P3, and T0P4 whose relative energies were predicted to be 54.1, 80, 79.2, and 82.9 kJ·mol^{-1}, respectively. The remaining products were generated by the addition reactions proceeding via T0/1, T0/2, T0/3, and T0/4 at the first steps to create IS1, IS2, IS3, and IS4, respectively, as can be seen in Figure 1. The M06-2X/6-311++G(3df,2p) optimized geometry of T0P1 (see Figure S3) indicates that the methyl group drags one H atom out of the NH_2 group of aniline at a distance of 1.368 Å, making the H−NH bond length stretch to 1.224 Å. The CH_3−H−NH abstraction is identified by the 1740i cm^{-1} imaginary frequency as shown in the T0P1 harmonic oscillator modes. The other H-abstraction processes were also found at the three transition states T0P2, T0P3, and T0P4 in which the first transition state (TS) abstracts H at the ortho-position, while the second and third TSs pull H out of the meta- and para-positions of the aniline compound. The breaking and forming bonds (C−H and CH_3−H) in the three TSs above optimized at the M06-2X/6-311++G(3df,2p) level are in the ranges of 1.37−1.38 and 1.28−1.30 Å, respectively. It can be seen from the PES that the abstraction channel leading to P1, $C_6H_5NH_2 + CH_3$ (RA) → T0P1 → P1, is found to be the most energetically and kinetically favorable channel; this channel is also a unique exothermic reaction pathway on the PES with the energy released by about 49 kJ·mol^{-1}. The three remaining abstraction channels, RA → T0P2/T0P3/T0P4 → P2/P3/P4, are considered to be endothermic processes with the energy absorbed ranging from 40.5 to 46.9 kJ·mol^{-1}.

The PES shows that from the reactants, the addition to the C1 position of aniline leads to intermediate IS1, which is connected

https://doi.org/10.1021/acsomega.3c01029
ACS Omega 2023, 8, 17005−17016

Table 1. Heats of Formation and Heats of Reaction ($\Delta H°_{298}$, in Units of kJ·mol^{-1}) of Some Species and 13 Reaction Channels in the $C_6H_5NH_2 + CH_3$ System Calculated at the CCSD(T)//M06-2X/6-311++G(3df,2p) Level of Theory in Comparison with the Experimental Data

species and reaction channels	CCSD(T)//M06-2X/6-311++G(3df,2p)[a]	experimental data
$C_6H_5NH_2$ (aniline)	86.20	87.03 ± 0.88[b]
CH_3 (methyl radical)	141.876	146.452 ± 0.055[c]
CH_4 (methane)	−74.012	−74.526 ± 0.049[c]
H (hydrogen atom)	213.581 ± 4.18	217.998 ± 0.000[c]
NH_2 (amino radical)	183.85 ± 4.18	186.03 ± 0.11[c]
C_6H_5NH (anilino radical)	251.426	251.217[d]
m-$C_6H_4NH_2$ (meta-amino phenyl radical)	341.941 ± 4.18	345.053[d]
$C_6H_5CH_3$ (toluene)	46.69 ± 4.18	50.11 ± 0.33[c]
o-CH_3-$C_6H_4NH_2$ (*ortho*-toluidine)	49.8 ± 4.18	53.2 ± 0.5[b]
m-CH_3-$C_6H_4NH_2$ (*meta*-toluidine)	51.96	61.1[b]
p-CH_3-$C_6H_4NH_2$ (*para*-toluidine)	51.85	41.8[b]
$C_6H_5NH_2 + CH_3 \rightarrow$ P1 ($C_6H_5NH + CH_4$)	−50.66	−56.80 ± 0.88[b,c,d]
$C_6H_5NH_2 + CH_3 \rightarrow$ P2 (*o*-$C_6H_4NH_2 + CH_4$)	43.66	n/a
$C_6H_5NH_2 + CH_3 \rightarrow$ P3 (*m*-$C_6H_4NH_2 + CH_4$)	39.85	37.04 ± 0.88[b,c,d]
$C_6H_5NH_2 + CH_3 \rightarrow$ P4 (*p*-$C_6H_4NH_2 + CH_4$)	46.22	n/a
$C_6H_5NH_2 + CH_3 \rightarrow$ P5 (*o*-CH_3-$C_6H_4NH_2$ + H)	35.31	37.72 ± 0.44[b,c]
$C_6H_5NH_2 + CH_3 \rightarrow$ P6 ($C_6H_4(H)CH_3 + NH_2$)	321.66	n/a
$C_6H_5NH_2 + CH_3 \rightarrow$ P7 ($H(CH_3)C_6H_3NH_2$ + H)	339.60	n/a
$C_6H_5NH_2 + CH_3 \rightarrow$ P8 (*m*-CH_3-$C_6H_4NH_2$ + H)	37.46	45.62 ± 0.94[b,c]
$C_6H_5NH_2 + CH_3 \rightarrow$ P9 ($C_6H_5CH_3 + NH_2$)	2.47	2.68 ± 0.46[b,c]
$C_6H_5NH_2 + CH_3 \rightarrow$ P10 (*p*-CH_3-$C_6H_4NH_2$ + H)	37.36	26.32 ± 0.94[b,c]
$C_6H_5NH_2 + CH_3 \rightarrow$ P11 ($C_6H_4CH_3 + NH_3$)	37.63	n/a
$C_6H_5NH_2 + CH_3 \rightarrow$ P12 (*m*-$H(CH_3)$-$C_6H_3 + NH_3$)	368.06	n/a
$C_6H_5NH_2 + CH_3 \rightarrow$ P13 (*p*-$H(CH_3)$-$C_6H_3 + NH_3$)	282.73	n/a

[a]Values in this work. [b]Values collected from NIST (webbook.nist.gov). [c]Values collected from active thermochemical tables (ATcT).[63,64] [d]Values collected from NIST-JANAF thermochemical tables.

via the T0/1 transition state located at 70.4 kJ·mol^{-1} above the entrance point; whereas the addition to the ortho-, meta- and para-positions of aniline gives rise to IS2, IS3, and IS4 intermediates, respectively. It is easy to see that the activation barrier of the first addition channel is about 16−22 kJ·mol^{-1} higher than those of the remaining addition channels, cf. Figure 1, showing that it is more difficult to form the IS1 intermediate state compared to the IS2−IS4 isomers. Among those species, IS2 is the most favorable intermediate in energy, while IS3 and IS4 intermediates have the same formation probability because the energy barriers of the channels RA → T0/3 → IS3 and RA → T0/3 → T0/4 are both equal to ∼54 kJ·mol^{-1}. In terms of thermodynamics, IS2 is also the most stable intermediate whose relative energy is about −50 kJ·mol^{-1}; however, the positions of IS1, IS3, and IS4 on the PES are respectively 32, 39, and 43 kJ·mol^{-1} below the starting point. After forming IS1−IS4 intermediates, various subreaction paths can occur via isomerization and/or dissociation processes resulting in different isomers, IS5−IS14, and/or diverse bimolecular products, P5−P13. It can be seen from the PES, that the four products, namely, P4, P8, P9, and P11, were produced when IS1 proceeded via the TSs T1P4, T1P8, T1P9, and T1P11 located 344, 249, 45, and 267 kJ·mol^{-1}, respectively, above the reactants. Apparently, the decomposition process IS1 → T1P9 → P9($C_6H_5CH_3 + NH_2$) is much advantageous than those of IS1 → T1P4 → P4(*p*-$C_6H_4NH_2 + CH_4$), IS1 → T1P8 → P8(*m*-CH_3-$C_6H_4NH_2$ + H), and IS1 → T1P11 → P11($C_6H_4CH_3 + NH_3$). Therefore, the P4, P8, and P11 products are expected to be tremendously hard to be created under ambient conditions. The P9 product is also more stable than the remaining ones; its relative energy is only 2 kJ·mol^{-1}, which is 45, 35.1, and 35.2 kJ·mol^{-1} lower than those of P4, P8, and P11, respectively. For the IS1 → T1P9 → P9 decomposition, the T1P9 transition state depicted a NH_2− abstract process by a lose bond of around 2.0 Å; this action was characterized by an imaginary frequency of 592i cm^{-1} calculated at the M06-2X/6-311++G(3df,2p) level, cf. Figure S3 and Table S2. From the IS2 intermediate state, there are various direct or indirect reaction paths leading to two bimolecular products P3(*m*-$C_6H_4NH_2 + CH_4$) and P5(*o*-CH_3-$C_6H_4NH_2$ + H), in which the first product was formed by the direct path, IS2 → P3, proceeding via the T2P3 saddle point located at the 368 kJ·mol^{-1} point on the PES. Due to the high energy barrier, this path can be ignored in any condition of the title reaction. As stated above, the RA → T0P3 → P3 channel also created the P3 product; considering the energy side, this channel is significantly more favorable than the IS2 → T2P3 → P3 channel. Therefore, it can be said that the P3 product was mainly produced by the abstraction channel. For the P5 product, it was formed by the direct channel IS2 → T2P5 → P5 and/or by the two indirect channels IS2 → T2/6 → T6P5 → P5 and IS2 → T2/12 → T12P5 → P5. It is worth noting that the direct channel consumes less energy than the two indirect channels (65 kJ·mol^{-1} at T2P5 vs 176 kJ·mol^{-1}) (T2/6 and 144 kJ·mol^{-1}) at T2/12; hence, the two indirect channels should not be utilized for the kinetic calculation in the latter section. The geometry of T2P5 shown in Figure S3 indicates that the abstraction of a H atom has a bond length of ∼1.8 Å; this transition state is confirmed by an imaginary frequency of 901i cm^{-1}. The PES also shows that the process forming the bimolecular product P5(*o*-CH_3-$C_6H_4NH_2$ + H) needs to receive at least 36 kJ·mol^{-1} from the environment. From the IS3 intermediate, three bimolecular products P2, P8, and P12 were produced, in

https://doi.org/10.1021/acsomega.3c01029
ACS Omega 2023, 8, 17005−17016

which P2(*o*-$C_6H_5NH_2$ + CH_4) and P12(*m*-H(CH_3)−C_6H_3 + NH_3) were made by the single channels IS3 → T3P2 → P2 and IS3 → T3/13 → IS13 → T13P12 → P12, while P8(*m*-CH_3−$C_6H_4NH_2$ + H) could be formed by various single and double channels, namely, IS3 → T3P8 → P8, IS3 → T3/10 → IS10 → T10P8 → P8, and IS3 → T3/11 → IS11 → T11P8 → P8. The channel yielding P2 describes the formation of CH_4 by the concerted elimination of H and CH_3 at the ortho- and para-positions of IS3; the bond distances of C_{ortho}−H and C_{para}−CH_3 recorded at the structure of T3P2 (see Figure S3) are 1.3 and 2.2 Å, which are distinguished by an imaginary frequency 1495i cm^{-1}. Considering the inherent barrier of ∼400 kJ·mol^{-1} with respect to IS3, the IS3 → P2 pathway via T3P2 cannot compete with the RA → P2 abstraction via T0P2, and the P2 is likely not formed by the decomposition. Among three reaction channels going to P8, the first path overcomes only one saddle point at the T3P8, whereas the second and third ones must cross two TSs for each channel. The T3P8 transition state shows a H-abstraction process of the C_{ortho}−H bond with the distance of 1.74 Å, cf. Figure S3, and the negative frequency of this vibration was found to be about 1023i cm^{-1}. Note that the inherent barrier of 48 kJ·mol^{-1} (T0/2) with respect to the separated reactants is lower than the addition barrier of 54 kJ·mol^{-1} (T0/3), while the relative energy of 65 kJ·mol^{-1} (T2P5) is also smaller than the energy of 71 kJ·mol^{-1} (T3P8) relative to the reactants, indicating that the endothermic reaction pathway yielding P8 (37 kJ·mol^{-1}) from the reactants does not compete with the channel RA → P5 (36 kJ·mol^{-1}). Considering the relative energies of T3P8 and T3/10 (140 kJ·mol^{-1}) and T3/11 (148 kJ·mol^{-1}), the first path is more favorable than the second and third paths; thus, the P8 product is mainly formed by the first channel. Unlike P2 and P8 products, P12(*m*-H(CH_3)−C_6H_3 + NH_3), was only produced by the fragmentation of IS3 → P12 via two tight exit transition states, T3/13 and T13P12, where the first-order saddle point T3/13 holds the highest energy level of 553 kJ·mol^{-1}. Furthermore, this product is also not stable in thermodynamics (367 kJ·mol^{-1}) relative to the reactants, suggesting that it is unlikely to be formed during the title reaction.

From the intermediate state IS4, six bimolecular products P2, P6, P7, P10, P11, and P13 can be formed, in which the P2, P6, P7, and P13 products were produced after forming intermediate state IS5 at 115 kJ·mol^{-1} by the IS4 → IS5 isomerization going via transition state T4/5 (295 kJ·mol^{-1}). The products P2(*o*-$C_6H_4NH_2$ + CH_4), P6(C_6H_4(H)CH_3 + NH_2), and P7(H-(CH_3)$C_6H_3NH_2$ + H) were formed directly via the corresponding saddle points T5P2 (399 kJ·mol^{-1}), T5P6 (329 kJ·mol^{-1}), and T5P7 (353 kJ·mol^{-1}), while the P13 product was formed indirectly through two TSs, namely, T5/9 (405 kJ·mol^{-1}) and T9P13 (322 kJ·mol^{-1}). It can be seen that the T4/5 transition state and all of the subsequent TSs are very high in energy, so the reaction paths leading to those products can be ignored when considering the mechanism of the title reaction. P11 was created by the two-step fragmentation IS4 → IS8 → P11 going via T4/8 (248 kJ·mol^{-1}) and T8P11 (141 kJ·mol^{-1}), whereas P10 was formed by two different channels IS4 → P10 via T4P10 (70.4 kJ·mol^{-1}) and IS4 → IS14 → P10 via T4/14 (149.5 kJ·mol^{-1}) and T14P10 (69 kJ·mol^{-1}). Apparently, only the direct channel IS4 → P10 is dominant in energy, which competes equally to the channel IS3 → P8 going via the T3P8 transition state located at 70.6 kJ·mol^{-1} above the reactants, guessing that the two channels RA → T0/3 → IS3 → T3P8 → P8 and RA → T0/4 → IS4 → T4P10 → P10 have the same reaction rate; however, they are both less favorable in comparison with the channel leading to the P5 product, RA → T0/2 → IS2 → T2P5.

It is not difficult to observe that the mechanism of the $C_6H_5NH_2$ + CH_3 reaction can be regarded as similar to that of the $C_6H_5CH_3$ + CH_3 reaction. An interesting aspect is that both CH_3 and NH_2 are type-I substituents, meaning they both donate electrons into the benzene aromatic ring, resulting in high electron density at the ortho- and para-positions. In the study of Li et al.,[57] the hydrogen abstraction mechanisms from toluene by the methyl radical were characterized carefully at the B3LYP/6-31G(2df,p) level of theory; the Gaussian-4(G4) composite method was also employed to achieve highly accurate thermochemical data. In this reaction system, the authors have indicated that hydrogen atoms can be abstracted either from the CH_3 group or from the ortho-, meta-, and para-positions. These abstraction channels proceeded via the transition states $TS_{CH_3-CH_3}$, TS_{CH_3-o}, TS_{CH_3-m}, and TS_{CH_3-p} whose barrier heights are 42.7, 68.2, 69.5, and 70.3 kJ·mol^{-1}, respectively. Meanwhile, the corresponding transition states T0P1, T0P2, T0P3, and T0P4 of the $C_6H_5NH_2$ + CH_3 reaction system, in this study, hold the barrier heights of 54.1, 80, 79.2, and 82.9 kJ·mol^{-1}. In terms of energy, it can be inferred that the hydrogen abstraction processes of the $C_6H_5CH_3$ + CH_3 reaction are more dominant than those of the $C_6H_5NH_2$ + CH_3 reaction. In addition, it can be seen that in both reaction systems, abstraction of hydrogen atoms from the methyl group of toluene and/or from the amine group of aniline is lower than that on the phenyl ring, and the differences between barrier heights for hydrogen abstraction at ortho-, meta-, and para-positions are less than 3 kJ·mol^{-1}. From the obtained barrier heights, we would expect that the difference between rate constants of H-abstraction by CH_3 from the methyl or amine groups and those from the phenyl ring will be more pronounced, while the difference in the reaction rate constants of H-abstraction by CH_3 from ortho-, meta-, and para-positions will be modest.

3.2. Thermochemical Properties. In order to check the accuracy of the calculations in this study, the enthalpy changes (ΔH°_{298K}) of some species such as $C_6H_5NH_2$, CH_3, CH_4, NH_2, C_6H_5NH, etc., and all of the reaction channels predicted at the CCSD(T)//M06-2X/6-311++G(3df,2p) level of theory were calculated and presented in Table 1. The available experimental data cited from the Active Thermochemical Tables (ATcT) and from NIST were also added in the table to compare with the calculated results. In general, as can be seen from Table 1, the calculated values are in good agreement with the literature values within their uncertainties (e.g., the maximum deviation between theory and experiment, in this case, is around 11 kJ·mol^{-1}). Such good agreement indicates that the methods, M06-2X and CCSD(T), used in the present study are absolutely reasonable.

In detail, it can be found that the most dominant channel, $C_6H_5NH_2$ + CH_3 → P1 (C_6H_5NH + CH_4), has the smallest value of the enthalpy change, which is about −50.7 kJ·mol^{-1} calculated at the CCSD(T) level. The deviation between this number with the experimental value for this channel is ∼6 kJ·mol^{-1}. Three reaction channels leading to isomer products, which are $C_6H_5NH_2$ + CH_3 → P2: *o*-$C_6H_4NH_2$ + CH_4, $C_6H_5NH_2$ + CH_3 → P3: *m*-$C_6H_4NH_2$ + CH_4, and $C_6H_5NH_2$ + CH_3 → P4: *p*-$C_6H_4NH_2$ + CH_4, have the same enthalpy changes, respectively, being 43.7, 39.9, and 46.2 kJ·mol^{-1} computed at the CCS3D(T) level. The calculated value of 39.9 kJ·mol^{-1} is found to be in good agreement with the experimental value of 37.04 ± 0.88 kJ·mol^{-1}, whereas the

https://doi.org/10.1021/acsomega.3c01029
ACS Omega 2023, 8, 17005−17016

Table 2. Rate Constants of the Reactions $C_6H_5NH_2 + CH_3 \rightarrow Px$ (x = 1−5, 8−10) at P = 760 Torr (Ar) and T = 300−2000 K

T	k_{a1}	k_{a2}	k_{a3}	k_{a4}	k_1	k_2	k_3	k_4
300	2.08×10^{-22}	2.24×10^{-42}	5.04×10^{-42}	8.62×10^{-43}	1.03×10^{-29}	1.62×10^{-30}	1.00×10^{-30}	5.30×10^{-31}
400	3.23×10^{-20}	4.45×10^{-39}	8.82×10^{-39}	2.19×10^{-39}	2.88×10^{-26}	7.21×10^{-27}	5.92×10^{-27}	2.35×10^{-27}
500	7.34×10^{-19}	4.81×10^{-37}	8.88×10^{-37}	2.75×10^{-37}	4.24×10^{-24}	1.39×10^{-24}	1.33×10^{-24}	4.53×10^{-25}
600	6.38×10^{-18}	1.20×10^{-35}	2.12×10^{-35}	7.57×10^{-36}	1.51×10^{-22}	6.00×10^{-23}	6.12×10^{-23}	2.00×10^{-23}
700	3.19×10^{-17}	1.29×10^{-34}	2.19×10^{-34}	8.69×10^{-35}	1.97×10^{-21}	8.56×10^{-22}	8.67×10^{-22}	3.01×10^{-22}
800	1.13×10^{-16}	8.10×10^{-34}	1.34×10^{-33}	5.74×10^{-34}	1.20×10^{-20}	5.54×10^{-21}	5.64×10^{-21}	2.06×10^{-21}
900	3.15×10^{-16}	3.54×10^{-33}	5.77×10^{-33}	2.61×10^{-33}	4.27×10^{-20}	2.13×10^{-20}	2.25×10^{-20}	8.15×10^{-21}
1000	7.43×10^{-16}	1.20×10^{-32}	1.92×10^{-32}	9.10×10^{-33}	1.08×10^{-19}	5.97×10^{-20}	6.68×10^{-20}	2.30×10^{-20}
1100	1.55×10^{-15}	3.34×10^{-32}	5.30×10^{-32}	2.61×10^{-32}	2.21×10^{-19}	1.38×10^{-19}	1.64×10^{-19}	5.26×10^{-20}
1200	2.92×10^{-15}	8.07×10^{-32}	1.27×10^{-31}	6.44×10^{-32}	4.05×10^{-19}	2.82×10^{-19}	3.57×10^{-19}	1.06×10^{-19}
1300	5.12×10^{-15}	1.74×10^{-31}	2.71×10^{-31}	1.41×10^{-31}	6.94×10^{-19}	5.36×10^{-19}	7.17×10^{-19}	1.99×10^{-19}
1400	8.44×10^{-15}	3.43×10^{-31}	5.29×10^{-31}	2.82×10^{-31}	1.14×10^{-18}	9.74×10^{-19}	1.37×10^{-18}	3.53×10^{-19}
1500	1.32×10^{-14}	6.26×10^{-31}	9.62×10^{-31}	5.23×10^{-31}	1.84×10^{-18}	1.72×10^{-18}	2.52×10^{-18}	6.07×10^{-19}
1600	1.99×10^{-14}	1.08×10^{-30}	1.64×10^{-30}	9.10×10^{-31}	2.95×10^{-18}	2.99×10^{-18}	4.57×10^{-18}	1.02×10^{-18}
1700	2.89×10^{-14}	1.76×10^{-30}	2.67×10^{-30}	1.50×10^{-30}	4.70×10^{-18}	5.18×10^{-18}	8.27×10^{-18}	1.69×10^{-18}
1800	4.06×10^{-14}	2.75×10^{-30}	4.16×10^{-30}	2.37×10^{-30}	7.57×10^{-18}	9.03×10^{-18}	1.51×10^{-17}	2.77×10^{-18}
1900	5.57×10^{-14}	4.14×10^{-30}	6.24×10^{-30}	3.60×10^{-30}	1.24×10^{-17}	1.60×10^{-17}	2.82×10^{-17}	4.56×10^{-18}
2000	7.46×10^{-14}	6.03×10^{-30}	9.06×10^{-30}	5.28×10^{-30}	2.07×10^{-17}	2.90×10^{-17}	5.33×10^{-17}	7.54×10^{-18}

measured data for the two remaining channels are not available (see Table 1).

The next three reaction channels, $C_6H_5NH_2 + CH_3 \rightarrow$ P5 (o-CH_3−$C_6H_4NH_2$ + H), $C_6H_5NH_2 + CH_3 \rightarrow$ P8 (m-CH_3-$C_6H_4NH_2$ + H), and $C_6H_5NH_2 + CH_3 \rightarrow$ P10 (p-CH_3-$C_6H_4NH_2$ + H), also hold the same values of 35.3, 37.5, and 37.4 kJ·mol^{-1}, respectively. The laboratory data collected from NIST (webbook.nist.gov), Active Thermochemical Tables (ATcT), and NIST-JANAF Thermochemical Tables for the corresponding channels are 37.72 ± 0.44, 45.62 ± 0.94, and 26.32 ± 0.94 kJ·mol^{-1}, showing that the maximum discrepancy between theory and experiment is about 11 kJ·mol^{-1}.

For the reaction channel $C_6H_5NH_2 + CH_3 \rightarrow$ P9 ($C_6H_5CH_3 + NH_2$), the enthalpy change is only 2.5 kJ·mol^{-1}, which agrees closely with the experimental value of 2.68 ± 0.46 kJ·mol^{-1}, indicating that the replacement process of the NH_2 group with the CH_3 group needs to receive very little energy from the environment. Among the last three reaction channels, namely, $C_6H_5NH_2 + CH_3 \rightarrow$ P11 ($C_6H_4CH_3 + NH_3$), $C_6H_5NH_2 + CH_3 \rightarrow$ P12 (m-H(CH_3)−C_6H_3 + NH_3), and $C_6H_5NH_2 + CH_3 \rightarrow$ P13 (p-H(CH_3)−C_6H_3 + NH_3), the first one owns the lowest enthalpy change of 37.63 kJ·mol^{-1}, while the two latter channels retain the values of 368 and 282.7 kJ·mol^{-1}, respectively, showing that the former consumes less energy than the two latter. The two products, P12 and P13, may not occur in ambient conditions. This statement is completely consistent with the conclusion in the energy analysis of the reactions on the PES. The agreement between the predicted values and the experimental data confirms that the methods used in this study are absolutely reliable.

3.3. Diagnostic and Spin Contamination Analysis. In this study, the T1 diagnostic analysis was also examined to approximately measure the multireference character in the wave function. The calculated values for all species involved depicted at the CCSD(T)/6-311++G(3df,2p) level are tabulated in Table S5. The table reveals that the T1 diagnostics for singlet-state and doublet-state species are less than 0.02 and 0.045, respectively, except for the two species m-H(CH_3)−C_6H_3 and p-H(CH_3)−C_6H_3 with the T1 diagnostics of 0.051 and 0.048, respectively (the threshold for the T1 diagnostic of a closed-shell species and an open-shell species was known to be 0.02 and 0.045, respectively),[58] indicating that the T1 diagnostics of all species do not have significant multireference characters. Although the T1 diagnostics for m-H(CH_3)−C_6H_3 and p-H(CH_3)−C_6H_3 produced incorrect energy values for these species, they were considered to be not critical to the title reaction; hence, it can be concluded that the single-reference methods can be surely utilized in this study. Furthermore, the analysis of spin contamination was also considered, and the results displayed in Table S5 indicate that the singlet states have $\langle S^2 \rangle$ values of 0.0, whereas the doublet states have values of ∼0.76, confirming that the impact of spin contamination on the determination of activation barriers and the structures of all species can be considered insignificant.

3.4. Rate Constant Calculations. As mentioned earlier, several reaction pathways depicted in Figure S1 with elevated energy barriers were not taken into account during the rate constant calculations as their impact on the overall product formation of the system was insignificant. Therefore, only the following reaction channels displayed in Figure 1 were considered to calculate rate constants for the second-order reaction $C_6H_5NH_2 + CH_3$

$$C_6H_5NH_2 + CH_3 \rightarrow \text{P1 } (C_6H_5NH + CH_4) \text{ via T0P1} \quad \text{(ka1)}$$

$$C_6H_5NH_2 + CH_3 \rightarrow \text{P2 } (o - C_6H_4NH_2 + CH_4) \text{ via T0P2} \quad \text{(ka2)}$$

$$C_6H_5NH_2 + CH_3 \rightarrow \text{P3 } (m - C_6H_4NH_2 + CH_4) \text{ via T0P3} \quad \text{(ka3)}$$

$$C_6H_5NH_2 + CH_3 \rightarrow \text{P4 } (p - C_6H_4NH_2 + CH_4) \text{ via T0P4} \quad \text{(ka4)}$$

$$C_6H_5NH_2 + CH_3 \rightarrow \text{IS1 via T0/1} \quad \text{(kb1)}$$

$$C_6H_5NH_2 + CH_3 \rightarrow \text{IS2 via T0/2} \quad \text{(kb2)}$$

$$C_6H_5NH_2 + CH_3 \rightarrow \text{IS3 via T0/3} \quad \text{(kb3)}$$

$$C_6H_5NH_2 + CH_3 \rightarrow \text{IS4 via T0/4} \quad \text{(kb4)}$$

https://doi.org/10.1021/acsomega.3c01029
ACS Omega 2023, 8, 17005−17016

$$C_6H_5NH_2 + CH_3 \rightarrow P5\ (o - CH_3{-}C_6H_4NH_2 + H) \quad (k1)$$

$$C_6H_5NH_2 + CH_3 \rightarrow P8\ (m - CH_3{-}C_6H_4NH_2 + H) \quad (k2)$$

$$C_6H_5NH_2 + CH_3 \rightarrow P9\ (C_6H_5CH_3 + NH_2) \quad (k3)$$

$$C_6H_5NH_2 + CH_3 \rightarrow P10\ (p - CH_3{-}C_6H_4NH_2 + H) \quad (k4)$$

Rate constants for the abstraction channels (k_{a1}−k_{a4}) and the addition channels (k_{b1}−k_{b4}) have been predicted by the transition state theory (TST), whereas those for the bimolecular reaction channels (k_1−k_4) have been calculated by the RRKM/ME approach. All rate-constant calculations were implemented by using the MESMER code[41] with the use of the Eckart tunneling effects.[46]

The calculated second-order rate constants k_{a1}−k_{a4} and k_1−k_4 in the temperature range of 300−2000 K and at 760 Torr (Ar) pressure for the channels $C_6H_5NH_2 + CH_3 \rightarrow$ (P1−P4) and $C_6H_5NH_2 + CH_3 \rightarrow$ (P5, P8, P9, and P10) are presented in Table 2, whereas the k_{b1}−k_{b4} rate coefficients for the $C_6H_5NH_2 + CH_3 \rightarrow C_7H_{10}N$ (IS1−IS4) channels are tabulated in Table 3.

Table 3. Rate Constants of the Reactions $C_6H_5NH_2 + CH_3 \rightarrow$ IS*x* (*x* = 1−4) at *P* = 760 Torr (Ar) and *T* = 300−2000 K

T	k_{b1}	k_{b2}	k_{b3}	k_{b4}
300	5.25×10^{-26}	3.50×10^{-21}	1.92×10^{-22}	2.55×10^{-22}
400	5.78×10^{-23}	3.61×10^{-19}	3.82×10^{-20}	4.96×10^{-20}
500	3.32×10^{-21}	6.11×10^{-18}	9.06×10^{-19}	1.17×10^{-18}
600	4.57×10^{-20}	3.78×10^{-17}	6.90×10^{-18}	8.80×10^{-18}
700	2.69×10^{-19}	1.24×10^{-16}	2.63×10^{-17}	3.32×10^{-17}
800	9.57×10^{-19}	2.70×10^{-16}	6.53×10^{-17}	8.10×10^{-17}
900	2.48×10^{-18}	4.51×10^{-16}	1.24×10^{-16}	1.50×10^{-16}
1000	5.22×10^{-18}	6.38×10^{-16}	1.98×10^{-16}	2.33×10^{-16}
1100	9.54×10^{-18}	8.19×10^{-16}	2.84×10^{-16}	3.25×10^{-16}
1200	1.58×10^{-17}	9.92×10^{-16}	3.82×10^{-16}	4.25×10^{-16}
1300	2.44×10^{-17}	1.16×10^{-15}	4.90×10^{-16}	5.35×10^{-16}
1400	3.59×10^{-17}	1.34×10^{-15}	6.12×10^{-16}	6.56×10^{-16}
1500	5.06×10^{-17}	1.53×10^{-15}	7.47×10^{-16}	7.91×10^{-16}
1600	6.90×10^{-17}	1.73×10^{-15}	8.97×10^{-16}	9.42×10^{-16}
1700	9.14×10^{-17}	1.94×10^{-15}	1.06×10^{-15}	1.11×10^{-15}
1800	1.18×10^{-16}	2.16×10^{-15}	1.24×10^{-15}	1.30×10^{-15}
1900	1.46×10^{-16}	2.39×10^{-15}	1.42×10^{-15}	1.51×10^{-15}
2000	1.76×10^{-16}	2.61×10^{-15}	1.60×10^{-15}	1.74×10^{-15}

The values of k_{a1}−k_{a4}, k_{b1}−k_{b4}, and k_1−k_4 over the 300−2000 K range and *P* = 76−76,000 Torr are shown in Tables S6−S11. The calculated temperature- and pressure-dependent rate constants and branching ratios for the main channels are graphically displayed in Figures 2−6.

The modified Arrhenius equations with three parameters adequately describes the calculated data in the temperature range of 300−2000 K at 760 Torr (Ar) pressure and can be given (in units of cm^3 $molecule^{-1}$ s^{-1}) as follows

$$k_{a1} = 7.5 \times 10^{-23}\ T^{3.04}\ \exp[(-40.63 \pm 0.29\ kJ{\cdot}mol^{-1})/RT]$$

$$k_{a2} = 7.95 \times 10^{-39}\ T^{3.21}\ \exp[(-65.98 \pm 0.17\ kJ{\cdot}mol^{-1})/RT]$$

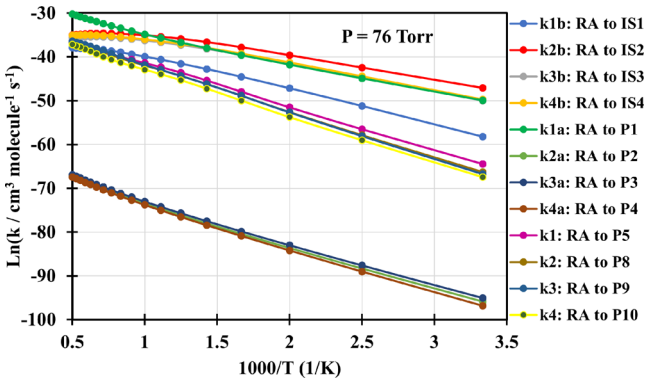

Figure 2. Plots of the predicted rate constants for the main reactions of the $C_6H_5NH_2 + CH_3$ system in the temperature range of 300−2000 K and at a pressure of 76 Torr Ar.

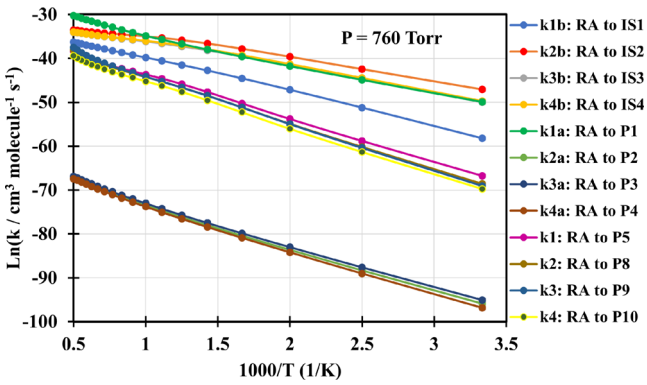

Figure 3. Plots of the predicted rate constants for the main reactions of the $C_6H_5NH_2 + CH_3$ system in the temperature range of 300−2000 K and at a pressure of 760 Torr Ar.

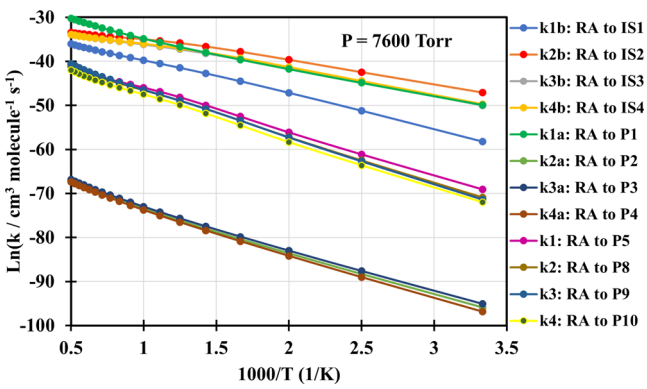

Figure 4. Plots of the predicted rate constants for the main reactions of the $C_6H_5NH_2 + CH_3$ system in the temperature range of 300−2000 K and at a pressure of 7600 Torr Ar.

$$k_{a3} = 9.74 \times 10^{-39}\ T^{3.23}\ \exp[(-64.73 \pm 0.29\ kJ{\cdot}mol^{-1})/RT]$$

$$k_{a4} = 9.28 \times 10^{-39}\ T^{3.19}\ \exp[(-68.49 \pm 0.29\ kJ{\cdot}mol^{-1})/RT]$$

$$k_{b1} = 1.59 \times 10^{-9}\ T^{-1.56}\ \exp[(-72.09 \pm 1.21\ kJ{\cdot}mol^{-1})/RT]$$

https://doi.org/10.1021/acsomega.3c01029
ACS Omega 2023, 8, 17005−17016

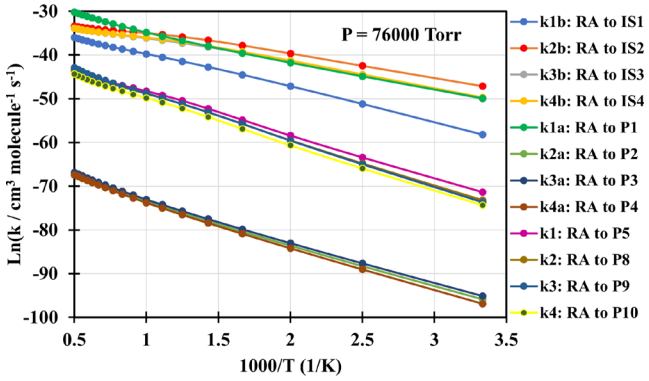

Figure 5. Plots of the predicted rate constants for the main reactions of the $C_6H_5NH_2 + CH_3$ system in the temperature range of 300−2000 K and at a pressure of 76,000 Torr Ar.

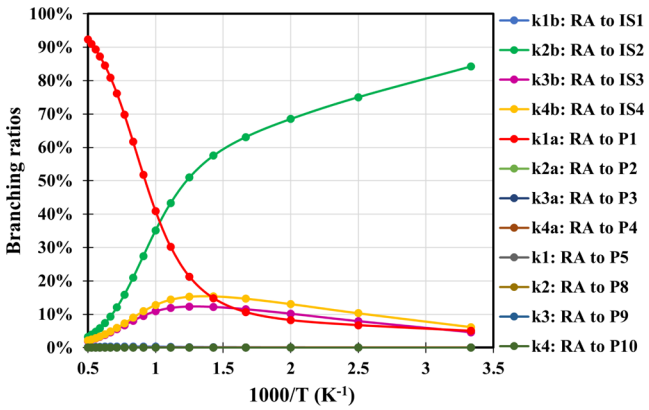

Figure 6. Branching ratios for the main channels of the $C_6H_5NH_2 + CH_3$ system in the temperature range of 300−2000 K and at 760 Torr (Ar) pressure. It should be noted that the branching ratios of some products (IS1, P2-P5, P8, P9) in this figure may not be visible due to their insignificant data. For more information, please refer to Table S14.

$$k_{b2} = 2.29 \times 10^{-3}\, T^{-3.19} \exp[(-56.94 \pm 1.17\ \text{kJ·mol}^{-1})/RT]$$

$$k_{b3} = 1.19 \times 10^{-5}\, T^{-2.54} \exp[(-60.21 \pm 1.09\ \text{kJ·mol}^{-1})/RT]$$

$$k_{b4} = 7.24 \times 10^{-5}\, T^{-2.77} \exp[(-60.71 \pm 1.30\ \text{kJ·mol}^{-1})/RT]$$

$$k_1 = 9.51 \times 10^{-15}\, T^{-0.22} \exp[(-83.09 \pm 2.68\ \text{kJ·mol}^{-1})/RT]$$

$$k_2 = 2.16 \times 10^{-18}\, T^{0.92} \exp[(-82.63 \pm 2.85\ \text{kJ·mol}^{-1})/RT]$$

$$k_3 = 4.88 \times 10^{-20}\, T^{1.49} \exp[(-82.22 \pm 3.05\ \text{kJ·mol}^{-1})/RT]$$

$$k_4 = 3.34 \times 10^{-17}\, T^{0.42} \exp[(-85.48 \pm 2.34\ \text{kJ·mol}^{-1})/RT]$$

$$k_{total} = 7.71 \times 10^{-17}\, T^{1.20} \exp[(-40.96 \pm 2.18\ \text{kJ·mol}^{-1})/RT]$$

Overall, it is observed that the rate constants for the designated reaction channels tend to increase with increasing temperature in the range of 300−2000 K, in which the most significant increase in rate constants can be seen in the values of k_{2a}, k_{3a}, k_{4a}, and k_1−k_4. The rate constant k_{2b} of the $C_6H_5NH_2 + CH_3 \rightarrow$ IS2 channel is the highest if the temperature is less than or equal to 900 K with the branching ratio over the range of 43−84% (T = 300−900, P = 760 Torr). In contrast, the k_{1a} value of the $C_6H_5NH_2 + CH_3 \rightarrow$ P1 ($C_6H_5NH + CH_4$) channel will occupy the first place if T > 900 K with the branching ratio of 30−92% (T = 900−2000 K, P = 760 Torr), cf. Figures 2−6. For example, the rate constants at (T = 300 K, P = 760 Torr) of k_{1a} and k_{2b} are 2.08×10^{-22} and 3.50×10^{-21} cm^3 molecule^{-1} s^{-1}, respectively, while those values at (T = 2000 K, P = 760 Torr) correspond to 7.46×10^{-14} and 2.61×10^{-15} cm^3 molecule^{-1} s^{-1}. Despite the sharp increase in value as mentioned above, the rate constants k_{2a}, k_{3a}, and k_{4a} of the reaction channels $C_6H_5NH_2 + CH_3 \rightarrow$ P2 (o-$C_6H_4NH_2 + CH_4$), $C_6H_5NH_2 + CH_3 \rightarrow$ P3 (m-$C_6H_4NH_2 + CH_4$), and $C_6H_5NH_2 + CH_3 \rightarrow$ P4 (p-$C_6H_4NH_2 + CH_4$) still hold the lowest values in comparison with the others, ranging from ∼10^{-42} to ∼10^{-30} cm^3 molecule^{-1} s^{-1} (T = 300−2000 K). The remaining rate constants k_1−k_4 of the reaction routes $C_6H_5NH_2 + CH_3 \rightarrow$ P5 (o-CH_3−$C_6H_4NH_2$ + H), $C_6H_5NH_2 + CH_3 \rightarrow$ P8 (m-CH_3−$C_6H_4NH_2$ + H), $C_6H_5NH_2 + CH_3 \rightarrow$ P9 ($C_6H_5CH_3 + NH_2$), and $C_6H_5NH_2 + CH_3 \rightarrow$ P10 (p-CH_3−$C_6H_4NH_2$ + H) occupy moderate values compared to the others, being about ∼10^{-30} to ∼10^{-17} cm^3 molecule^{-1} s^{-1}, with the total branching ratio being less than 1% (T = 900−2000 K, P = 760 Torr). It should be noted that the calculated rate constants for each channel on the PES are completely consistent with the above-analyzed results in energy.

It is worth noting that the effect of pressure on the rate constants has also been considered in the present study. From Tables 2, 3, and S6−S11, it can be seen that the k_{1a}−k_{4a} rate constants are pressure-independent values. These calculated results are completely reasonable because all of the four abstraction channels (k_{1a})−(k_{4a}) are elementary reactions, in which each of them overcomes only one transition state as discussed above. The k_{1b}−k_{4b} rate constants were recorded to slightly increase with an increase of pressure in the 7.6−76,000 Torr range and in the case of T > 300 K. At T = 300 K, those values are independent of the pressure. If going into specific conditions, it is easy to realize that at the conditions of ($T \leq 400$ K and $760 \leq P \leq 7600$ Torr) or ($T \leq 800$ K and $7600 \leq P \leq$ 76,000 Torr), the k_{1b} values do not depend on the pressure; e.g., the 400 K rate constant of k_{1b} is 5.78×10^{-23} cm^3 molecule^{-1} s^{-1} at both the pressure numbers of 760 and 7600 Torr. At the conditions of ($T \leq 400$ K and $76 \leq P \leq 760$ Torr), ($T \leq 700$ K and $760 \leq P \leq 7600$ Torr), or ($T \leq 900$ K and $7600 \leq P \leq$ 76,000 Torr), the effect of pressure on the k_{2b} values can be ignored. Similar signs have also been found in the condition ranges of ($T \leq 400$ K and $76 \leq P \leq 760$ Torr), ($T \leq 600$ K and $760 \leq P \leq 7600$ Torr), or ($T \leq 1000$ K and $7600 \leq P \leq 76{,}000$ Torr) for the values of k_{3b} and ($T \leq 400$ K and $76 \leq P \leq 760$ Torr), ($T \leq 600$ K and $760 \leq P \leq 7600$ Torr), or ($T \leq 1100$ K and $7600 \leq P \leq 76{,}000$ Torr) for the values of k_{4b}, cf. Tables 2,3, and S6−S11. Unlike the k_{1b}−k_{4b} rate constants, the k_1−k_4 values tend to reduce steadily as the pressure increases. For instance, the 300 K values of k_1 at P = 76, 760, 7600, and 76,000 Torr were

https://doi.org/10.1021/acsomega.3c01029
ACS Omega 2023, 8, 17005−17016

predicted to be 1.03×10^{-28}, 1.03×10^{-29}, 1.03×10^{-30}, and 1.03×10^{-31} cm^3 $molecule^{-1}$ s^{-1}, respectively; the 1000 K rate constants of k_2 were 5.88×10^{-19}, 5.97×10^{-20}, 5.97×10^{-21}, and 5.97×10^{-22} cm^3 $molecule^{-1}$ s^{-1} calculated at P = 76, 760, 7600, and 76,000 Torr, respectively. Although the k_1−k_4 values decrease with increasing pressures, the total rate constant of the title reaction system still increases as the pressure increases in the range of 76−76,000 Torr (see Table S12 and Figure 7). This can be explained by the very weak decrease of the k_1−k_4 values compared with the strong increase of the k_{1a}−k_{4a} data.

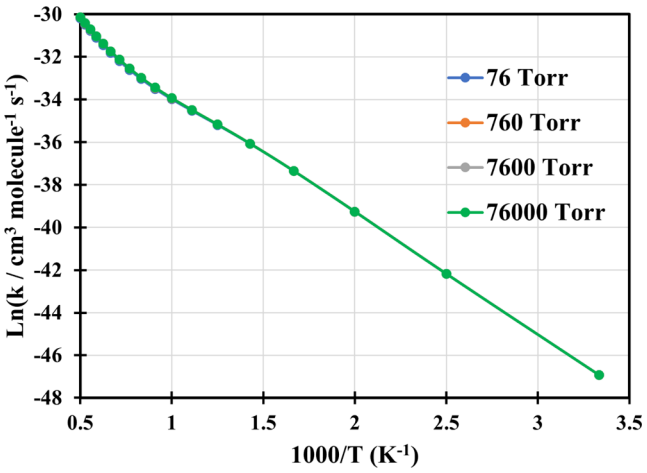

Figure 7. Plots of the predicted total rate constants of the $C_6H_5NH_2$ + CH_3 system in the temperature range of 300−2000 K and at different pressures of 76−76,000 Torr Ar. It should be noted that the invisibility of the kinetic lines at 76, 760, and 7600 Torr should be acknowledged because the calculated values at these pressures exhibit only minor differences as can be seen in Table S15.

Furthermore, in order to evaluate the capability of the $C_6H_5NH_2$ + CH_3 reaction system, in this study, the calculated rate constants for the H-abstraction channels (k_{1a}−k_{4a}) have also been compared with those ($k_{CH_3-CH_3}$, $k_{CH_3\text{-}o}$, $k_{CH_3\text{-}m}$, $k_{CH_3\text{-}p}$) of the similar system, $C_6H_5CH_3$ + CH_3,[57] as shown in Table S13. From the table, it can be seen that the k_{1a}−k_{4a} values of the $C_6H_5NH_2$ + CH_3 reaction are much smaller than the respective values $k_{CH_3-CH_3}$, $k_{CH_3\text{-}o}$, $k_{CH_3\text{-}m}$, and $k_{CH_3\text{-}p}$ of the $C_6H_5CH_3$ + CH_3 reaction. Particularly, the k_{1a} number is approximately two orders of magnitude smaller than the $k_{CH_3-CH_3}$ number over the 300−2000 K temperature range, and the k_{2a}−k_{4a} values are about 18 orders of magnitude lower than the $k_{CH_3\text{-}o}$, $k_{CH_3\text{-}m}$, and $k_{CH_3\text{-}p}$ values at T = 300 K but the difference between them tends to slightly reduce to 17 orders of magnitude as the temperature reaches 2000 K. In both reaction systems, the deviation in reaction rate constants of H-abstraction by CH_3 from ortho-, meta-, and para-positions is negligible. Thus, it can be observed that the kinetic comparison results are also consistent with the energy comparison results mentioned in the previous section. This further confirms that the H-abstraction processes from the different positions of toluene by the methyl radical are much easier than those from the various sites of aniline.

Last but not the least, the rate constant of the CH_3 + $C_6H_5NH_2$ reaction should also be compared to that of the CH_3 + O_2 reaction to consider the relevance of the former for the atmospheric chemistry. It is not difficult to realize that molecular oxygen exists in the atmosphere with a very high concentration compared to aniline (~5.3×10^{18} molecule/cm^3 vs tens of pptv); thus, the density of oxygen is dominant relative to aniline density in the atmosphere. Also, in the air, the reaction of the CH_3 radical with molecular oxygen proceeds so fast with the rate constant at room temperature of ~1.2×10^{-14} cm^3 $molecule^{-1}$ s^{-1},[59] while, in this condition, the total rate constant of the reaction between aniline and CH_3 is only 4.2×10^{-21} cm^3 $molecule^{-1}$ s^{-1}. Therefore, it can be said that aniline cannot compete with the molecular oxygen in the reaction with the CH_3 radical unless this radical appears with such a high concentration (more than 6×10^{15} molecule/cm^3).[60] However, the interaction of CH_3 with O_2 is normally affected by inert gases such as N_2 or Ne in the atmosphere, leading to a third-order reaction (CH_3 + O_2 + M → CH_3OO + M, M = N_2 or Ne) with the rate constant of only 1.6×10^{-31} [(cm^3/molecule)^2 s^{-1}][61] or 1.35×10^{-31} [(cm^3/molecule)^2 s^{-1}];[62] in this case, the CH_3 + $C_6H_5NH_2$ reaction is apparently much faster than the CH_3 + O_2 + M reaction. Thus, it can be said that these two reactions can compete with each other, depending on different influencing factors.

4. CONCLUDING REMARKS

In the present study, the quantum chemical approach has been applied to investigate the mechanism, kinetics, thermochemical properties, as well as diagnostic and spin contamination analysis of the $C_6H_5NH_2$ + CH_3 reaction system. All of the species of the system including the reactants, intermediate states, transition states, and products have been optimized by the M06-2X method in conjunction with the basis set 6-311++G(3df,2p). The single-point energy values of the substances displayed on the PES have been calculated by the very expensive method, CCSD(T), with the same basis set above.

The mechanism of the $C_6H_5NH_2$ + CH_3 reaction can take place as the addition style and/or the abstraction style. In the first direction, the system proceeds via four well-defined transition states T0/1, T0/2, T0/3, and T0/4 to form the stable intermediates, namely, IS1, IS2, IS3, and IS4 located 32, 49.8, 38.7, and 43.1 kJ·mol^{-1} below the reactants. In the second direction, the system proceeds through four saddle points T0P1, T0P2, T0P3, and T0P4 to generate the corresponding bimolecular products P1, P2, P3, and P4. The calculated results also revealed that the most dominant channels are the addition path $C_6H_5NH_2$ + CH_3 → IS2 going via T0/2 and the abstraction channel $C_6H_5NH_2$ + CH_3 → P1 proceeding via T0P1. These two channels compete with each other in energy.

The predicted enthalpy changes ($\Delta H°_{298K}$) of some species such as $C_6H_5NH_2$, CH_3, CH_4, NH_2, C_6H_5NH as well as the heats of the reaction paths leading to the P1−P13 products were predicted at the CCSD(T)//M06-2X/6-311++G(3df,2p) level of theory. The calculated values are satisfactory with the available experimental data within their uncertainties (the maximum deviation between theory and experiment is ~11 kJ·mol^{-1}). Such good agreement confirms that the methods used in this work are reliable and the calculated energies can be utilized to compute rate constants for the title reaction. The calculation results for T1 diagnostics and the spin contamination indicated that the T1 diagnostics of all species do not have significant multireference character and the spin contamination effect can be ignored.

The rate constants of the main channels are highly temperature-dependent. Specifically, the k_{2b} value of the $C_6H_5NH_2$ + CH_3 → IS2 channel exhibits the highest at T < 900 K, whereas the k_{1a} value of the $C_6H_5NH_2$ + CH_3 → P1

https://doi.org/10.1021/acsomega.3c01029
ACS Omega 2023, 8, 17005−17016

($C_6H_5NH + CH_4$) channel exhibits the highest at $T > 900$ K. Although the rate constants k_{2a}, k_{3a}, and k_{4a} rapidly increase with increasing temperature, they remain the lowest in the given temperature region, being $\sim 10^{-42}$ to $\sim 10^{-30}$ cm^3 $molecule^{-1}$ s^{-1}. Compared to the others, the rate constants k_1-k_4 are of moderate magnitude, being $\sim 10^{-30}$ to $\sim 10^{-17}$ cm^3 $molecule^{-1}$ s^{-1}, and they show a consistent decrease as the pressure increases. The $k_{1a}-k_{4a}$ values are pressure-independent, whereas the $k_{1b}-k_{4b}$ values were observed to exhibit a slight increase with increasing pressure within the range of 76−76,000 Torr and $T >$ 300 K. The total rate constant of the title reaction generally increases as the pressure increases. Additionally, in this study, the reaction rate constant of $CH_3 + O_2$ has been compared with that of the title reaction. It was observed that in air, the bimolecular reaction $CH_3 + O_2$ occurs rapidly compared to the $C_6H_5NH_2 + CH_3$ reaction. However, the third-order reaction ($CH_3 + O_2 + M \rightarrow CH_3OO + M$, where M = N_2 or Ne) was found to proceed slowly in comparison to the $C_6H_5NH_2 + CH_3$ reaction. Therefore, it can be concluded that the reaction between aniline and the methyl radical can proceed fully in the atmospheric environment, despite the presence of molecular oxygen at high concentrations.

The results of this study are crucial for comprehending the mechanism and kinetics of the reaction between $C_6H_5NH_2$ and the CH_3 radical. Considering the species produced by the title reaction, the main species (namely, product P1 and intermediate IS2, cf. Figure 1) should be included in any photolysis-related model under atmospheric conditions. In addition, the dominant intermediate product, IS2 (2-methyl-aniline), of the title reaction produced at temperatures below 900 K can help us somewhat understand the chemistry of aniline (the simplest aromatic compound containing nitrogen) under the attack of the methyl radical in the troposphere.

■ ASSOCIATED CONTENT

Supporting Information

The Supporting Information is available free of charge at https://pubs.acs.org/doi/10.1021/acsomega.3c01029.

Single-point energies and zero-point vibrational energies (ZPVE) of the reactants, intermediates, transition states, and products of the $C_7H_{10}N$ system at the M06-2X/6-311++G(3df,2p) and CCSD(T)/6-311++G(3df,2p) levels of theory; frequencies of reactants, intermediates, transition states, and products of the $C_6H_5NH_2 + CH_3$ reaction at the M06-2X/6-311++G(3df,2p) level; optimized coordinates of reactants, intermediates, transition states, and products of the $C_6H_5NH_2 + CH_3$ reaction at the M06-2X/6-311++G(3df,2p) level of theory; Gibbs free energies (ΔG_{298K}) and entropies (ΔS_{298K}) in $J \cdot mol^{-1}K^{-1}$ of the $C_7H_{10}N$ system at 298 K, and ΔG_{298K} and ΔS_{298K} were calculated at CCSD(T)/6-311++G(3df,2p) and M06-2X/6-311++G(3df,2p) levels, respectively; results of T1 diagnostic analysis and spin contamination $\langle S^2 \rangle$ for most of the species on the PES of the $C_6H_5NH_2 + CH_3$ system implemented at the CCSD(T)/6-311++G(3df,2p) level of theory; rate constants of the reactions $C_6H_5NH_2 + CH_3 \rightarrow Px$ (x = 1−5, 8−10) at P = 76−76,000 Torr (Ar) and T = 300−2000 K; rate constants of the reactions $C_6H_5NH_2 + CH_3 \rightarrow ISx$ (x = 1−4) at P = 76−76,000 Torr (Ar) and T = 300−2000 K; branching ratios for the main channels of the $C_6H_5NH_2 + CH_3$ system in the temperature range of 300−2000 K and at 760 Torr (Ar) pressure; the predicted total rate constants of the $C_6H_5NH_2 + CH_3$ system in the temperature range of 300−2000 K and at different pressures of 76−76,000 Torr Ar; and geometries of the reactants, intermediate states, transition states, and products optimized at the M06-2X/6-311++G(3df,2p) level (PDF)

■ AUTHOR INFORMATION

Corresponding Authors

Tien V. Pham − *School of Chemical Engineering, Hanoi University of Science and Technology, Hanoi 100000, Vietnam*; orcid.org/0000-0002-2067-9028; Email: tien.phamvan@hust.edu.vn

Hoang T. T. Trang − *Department of Chemistry, Hanoi Architectural University, Hanoi 100000, Vietnam*; Email: tranghtt29@gmail.com

Complete contact information is available at: https://pubs.acs.org/10.1021/acsomega.3c01029

Notes

The authors declare no competing financial interest.

■ ACKNOWLEDGMENTS

This research is funded by the Hanoi University of Science and Technology (HUST) under Grant Number T2022-PC-069. The authors acknowledge the National Center for High-Performing Computers in Taiwan for the use of its facility.

■ REFERENCES

(1) Palmiotto, G.; Pieraccini, G.; Moneti, G.; Dolara, P. Determination of the levels of aromatic amines in indoor and outdoor air in Italy. *Chemosphere* **2001**, *43*, 355−361.

(2) Anjalin, M.; Kanagathara, N.; Suganthi, A. R. B. A brief review on aniline and its derivatives. *Mater. Today: Proc.* **2020**, *33*, 4751−4755.

(3) Khan, M. F.; Wu, X.; Kaphalia, B. S.; Boor, P. J.; Ansari, G. A. S. Acute hematopoietic toxicity of aniline in rats. *Toxicol. Lett.* **1997**, *92*, 31−37.

(4) Khan, M. F.; Wu, X.; Kaphalia, B. S.; Boor, P. J.; Ansari, G. A. Nitrotyrosine formation in splenic toxicity of aniline. *Toxicology* **2003**, *194*, 95−102.

(5) Shahrezaei, F.; Mansouri, Y.; Zinatizadeh, A. A. L.; Akhbari, A. Photocatalytic Degradation of Aniline Using TiO_2 Nanoparticles in a Vertical Circulating Photocatalytic Reactor. *Int. J. Photoenergy* **2012**, *2012*, 1−8.

(6) Xie, H. B.; Ma, F.; Wang, Y.; He, N.; Yu, Q.; Chen, J. Quantum Chemical Study on Cl-Initiated Atmospheric Degradation of Monoethanolamine. *Environ. Sci. Technol.* **2015**, *49*, 13246−13255.

(7) Xie, H. B.; Ma, F.; Yu, Q.; He, N.; Chen, J. Computational Study of the Reactions of Chlorine Radicals with Atmospheric Organic Compounds Featuring NH_x-π-Bond (x = 1, 2) Structures. *J. Phys. Chem. A* **2017**, *121*, 1657−1665.

(8) Onel, L.; Dryden, M.; Blitz, M. A.; Seakins, P. W. Atmospheric Oxidation of Piperazine by OH has a Low Potential To Form Carcinogenic Compounds. *Environ. Sci. Technol. Lett.* **2014**, *1*, 367−371.

(9) Onel, L.; Blitz, M.; Dryden, M.; Thonger, L.; Seakins, P. Branching ratios in reactions of OH radicals with methylamine, dimethylamine, and ethylamine. *Environ. Sci. Technol.* **2014**, *48*, 9935−9942.

(10) Karl, M.; Svendby, T.; Walker, S. E.; Velken, A. S.; Castell, N.; Solberg, S. Modelling atmospheric oxidation of 2-aminoethanol (MEA) emitted from post-combustion capture using WRF-Chem. *Sci. Total Environ.* **2015**, *527*−*528*, 185−202.

(11) Nielsen, C. J.; Herrmann, H.; Weller, C. Atmospheric chemistry and environmental impact of the use of amines in carbon capture and storage (CCS). *Chem. Soc. Rev.* **2012**, *41*, 6684−6704.

(12) da Silva, G. Formation of nitrosamines and alkyldiazohydroxides in the gas phase: the CH_3NH + NO reaction revisited. *Environ. Sci. Technol.* **2013**, *47*, 7766−7772.
(13) Tang, Y.; Nielsen, C. J. A systematic theoretical study of imines formation from the atmospheric reactions of R_nNH_{2-n} with O_2 and NO_2 (R = CH_3 and CH_3CH_2; n = 1 and 2). *Atmos. Environ.* **2012**, *55*, 185−189.
(14) Turkevich, J.; Fujita, Y. Methyl radicals: preparation and stabilization. *Science* **1966**, *152*, 1619−1621.
(15) Kohse-Höinghaus, K.; Oßwald, P.; Cool, T. A.; Kasper, T.; Hansen, N.; Qi, F.; Westbrook, C. K.; Westmoreland, P. R. Biofuel combustion chemistry: from ethanol to biodiesel. *Angew. Chem., Int. Ed.* **2010**, *49*, 3572−3597.
(16) Wang, Z.; Zeng, D.; Patrick, W. H. Methane emissions from natural wetlands. *Environ. Monit. Assess.* **1996**, *42*, 143−161.
(17) Basco, N.; James, D. G. L.; James, F. C. A quantitative study of alkyl radical reactions by kinetic spectroscopy. II. Combination of the methyl radical with the oxygen molecule. *J. Chem. Kinet.* **1972**, *4*, 129−149.
(18) Zhang, J. X.; Liu, J. Y.; Li, Z. S.; Sun, C. C. Theoretical study on the reaction mechanism of the methyl radical with nitrogen oxides. *J. Comput. Chem.* **2005**, *26*, 807−817.
(19) Zhu, R.; Lin, M. C. The CH_3 + HO_2 Reaction: First-Principles Prediction of Its Rate Constant and Product Branching Probabilities. *J. Phys. Chem. A* **2001**, *105*, 6243−6248.
(20) Albaladejo, J.; Jiménez, E.; Notario, A.; Cabañas, B.; Martínez, E. CH_3O Yield in the CH_3 + O_3 Reaction Using the LP/LIF Technique at Room Temperature. *Phys. Chem. A* **2002**, *106*, 2512−2519.
(21) Hsu, D. S. Y.; Shaub, W. M.; Creamer, T.; Gutman, D.; Lin, M. C. Kinetic Modeling of CO Production from the Reaction of CH_3 with O_2 in Shock Waves. *Ber. Bunsenges. Phys. Chem.* **1983**, *87*, 909−919.
(22) Mellouki, A.; Le Bras, G.; Sidebottom, H. Kinetics and mechanisms of the oxidation of oxygenated organic compounds in the gas phase. *Chem. Rev.* **2003**, *103*, 5077−5096.
(23) Alvarez, E. G.; Amedro, D.; Afif, C.; Gligorovski, S.; Schoemaecker, C.; Fittschen, C.; Doussin, J. F.; Wortham, H. Unexpectedly high indoor hydroxyl radical concentrations associated with nitrous acid. *Proc. Natl. Acad. Sci. U.S.A.* **2013**, *110*, 13294−13299.
(24) Finlayson-Pitts, B. J.; Pitts, J. N., Jr. *Atmospheric Chemistry: Fundamentals and Experimental Techniques*; Wiley: New York, 1986.
(25) Lindstedt, P.; Robinson, R.; Allan, R.; Filip, S. V. In *Hydrogen Abstraction from the Amine Group of Aniline*, Conference: Chemical Kinetics, Seville Spain, 2013.
(26) Zhao, Y.; Truhlar, D. G. A New Local Density Functional for Main-Group Thermochemistry, Transition Metal Bonding, Thermochemical Kinetics, and Noncovalent Interactions. *J. Chem. Phys.* **2006**, *125*, No. 194101.
(27) Zhao, Y.; Truhlar, D. G. Density Functional for Spectroscopy: No Long-Range Self-Interaction Error, Good Performance for Rydberg and Charge-Transfer States, and Better Performance on Average than B3LYP for Ground States. *J. Phys. Chem. A* **2006**, *110*, 13126−13130.
(28) Zhao, Y.; Truhlar, D. G. The M06 Suite of Density Functionals for Main Group Thermochemistry, Thermochemical Kinetics, Noncovalent Interactions, Excited States, and Transition Elements. *Theory Chem. Acc.* **2008**, *120*, 215−241.
(29) Scuseria, G. E.; Janssen, C. L.; Schaefer III, H. F. An efficient reformulation of the closed-shell coupled cluster single and double excitation (CCSD) equations. *J. Chem. Phys.* **1988**, *89*, 7382−7387.
(30) Bartlett, R. J.; Musial, M. Coupled-cluster theory in quantum chemistry. *Rev. Mod. Phys.* **2007**, *79*, 291−352.
(31) Alecu, I. M.; Zheng, J.; Zhao, Y.; Truhlar, D. G. Computational Thermochemistry: Scale Factor Databases and Scale Factors for Vibrational Frequencies Obtained from Electronic Model Chemistries. *J. Chem. Theory Comput.* **2010**, *6*, 2872−2887.
(32) Pham, T. V.; Trang, H. T. T. Theoretical Investigation of the Mechanisms and Kinetics of the Bimolecular and Unimolecular Reactions Involving in the C_4H_6 Species. *J. Phys. Chem. A* **2021**, *125*, 585−596.
(33) Pham, T. V.; Trang, H. T. T. Combination Reactions of Propargyl Radical with Hydroxyl Radical and the Isomerization and Dissociation of trans-Propenal. *J. Phys. Chem. A* **2020**, *124*, 6144−6157.
(34) Pham, T. V. Theoretical Investigation on Mechanism, Thermochemistry, and Kinetics of the Gas-phase Reaction of 2-Propargyl Radical with Formaldehyde. *Chem. Res. Chin. Univ.* **2019**, *35*, 884−891.
(35) Pham, T. V.; Trang, H. T. T.; Trinh, L. H.; Tue, N. N. Theoretical Study of the Kinetics of the Gas-Phase Reaction between Phenyl and Amino Radicals. *ACS Omega* **2020**, *5*, 1277−1286.
(36) Pham, T. V.; Trang, H. T. T.; Nguyen, H. M. T. Temperature and Pressure-Dependent Rate Constants for the Reaction of the Propargyl Radical with Molecular Oxygen. *ACS Omega* **2022**, *7*, 33470−33481.
(37) Chen, H. T.; Pham, T. V.; Lin, M. C. Computational study on the mechanisms and rate constants for the O (^{3}P, ^{1}D) + OCS reactions. *J. Phys. Chem. A* **2019**, *123*, 8358−8364.
(38) Gonzalez, C.; Schlegel, H. B. An improved algorithm for reaction path following. *J. Chem. Phys.* **1989**, *90*, 2154−2161.
(39) Gonzalez, C.; Schlegel, H. B. Reaction path following in mass-weighted internal coordinates. *J. Chem. Phys.* **1990**, *94*, 5523−5527.
(40) Frisch, M. J.; Trucks, G. W.; Schlegel, H. B.; Scuseria, G. E.; Robb, M. A.; Cheeseman, J. R.; Scalmani, G.; Barone, V.; Petersson, G. A.; Nakatsuji, H.; Li, X.; Caricato, M.; Marenich, A.; Bloino, J.; Janesko, B. G.; Gomperts, R.; Mennucci, B.; Hratchian, H. P.; Ortiz, J. V.; Izmaylov, A. F.; Sonnenberg, J. L.; Williams-Young, D.; Ding, F.; Lipparini, F.; Egidi, F.; Goings, J.; Peng, B.; Petrone, A.; Henderson, T.; Ranasinghe, D.; Zakrzewski, V. G.; Gao, J.; Rega, N.; Zheng, G.; Liang, W.; Hada, M.; Ehara, M.; Toyota, K.; Fukuda, R.; Hasegawa, J.; Ishida, M.; Nakajima, T.; Honda, Y.; Kitao, O.; Nakai, H.; Vreven, T.; Throssell, K.; Montgomery, J. A.; Peralta, J. E.; Ogliaro, F.; Bearpark, M.; Heyd, J. J.; Brothers, E.; Kudin, K. N.; Staroverov, V. N.; Keith, T.; Kobayashi, R.; Normand, J.; Raghavachari, K.; Rendell, A.; Burant, J. C.; Iyengar, S. S.; Tomasi, J.; Cossi, M.; Millam, J. M.; Klene, M.; Adamo, C.; Cammi, R.; Ochterski, J. W.; Martin, R. L.; Morokuma, K.; Farkas, O.; Foresman, J. B.; Fox, D. J. *Gaussian 16*; Gaussian, Inc.: Wallingford CT, USA, 2016.
(41) Glowacki, D. R.; Liang, C. H.; Morley, C.; Pilling, M. J.; Robertson, S. H. MESMER: an open-source master equation solver for multi-energy well reactions. *J. Phys. Chem. A* **2012**, *116*, 9545−9560.
(42) Eyring, H. The activated complex in chemical reactions. *J. Chem. Phys.* **1935**, *3*, 107−115.
(43) Klippenstein, S. J. Variational optimizations in the Rice−Ramsperger−Kassel−Marcus theory calculations for unimolecular dissociations with no reverse barrier. *J. Chem. Phys.* **1992**, *96*, 367−371.
(44) Klippenstein, S. J. A bond length reaction coordinate for unimolecular reactions. II. Microcanonical and canonical implementations with application to the dissociation of NCNO. *J. Chem. Phys.* **1991**, *94*, 6469−6482.
(45) Holbrook, K. A.; Pilling, M. J.; Robertson, S. H. *Unimolecular Reactions*; J. Wiley: Chichester, UK, 1996
(46) Eckart, C. The penetration of a potential barrier by electrons. *Phys. Rev.* **1930**, *35*, 1303−1309.
(47) Hue, M. T. N.; Pham, T. V.; Hung, V. H.; Pham, T. H.; Ngo, T. C. Mechanism and kinetics of the reaction of the 2-propargyl radical with ammonia. *Int. J. Chem. Kinet.* **2019**, *52*, 84−91.
(48) Lanfri, L.; Wang, Y. L.; Pham, T. V.; Nguyen, N. T.; Paci, M. B.; Lin, M. C.; Lee, Y. P. Infrared Emission from Photodissociation of Methyl Formate [$HC(O)OCH_3$] at 248 and 193 nm: Absence of Roaming Signature. *J. Phys. Chem. A* **2019**, *123*, 6130−6143.
(49) Pham, T. V.; Trang, H. T. T.; Ngo, C. T.; Nguyen, H. M. T. A quantum chemical study of the mechanisms and kinetics of the reaction between propargyl (C_3H_3) and methyl (CH_3) radicals. *Chem. Phys. Lett.* **2021**, *762*, No. 138126.
(50) Pham, T. V.; Trang, H. T. T. A theoretical study on mechanism and kinetics of the C_2H_3 + C_2H_3 recombination and the isomerization and dissociation of butadiene. *Chem. Phys.* **2021**, *548*, No. 111217.
(51) Van Pham, T.; Tue, N. N.; Trang, H. T. T. Computational Investigation on the Formation and Decomposition Reactions of the C_4H_3O compound. *ACS Omega* **2021**, *6*, 17965−17976.

https://doi.org/10.1021/acsomega.3c01029
ACS Omega 2023, 8, 17005−17016

(52) Miller, J. A.; Klippenstein, S. J. The recombination of propargyl radicals: Solving the master equation. *J. Phys. Chem. A* **2001**, *105*, 7254−7266.
(53) Hippler, H.; Troe, J.; Wendelken, H. J. Collisional deactivation of vibrationally highly excited polyatomic molecules. II. Direct observations for excited toluene. *J. Chem. Phys.* **1983**, *78*, 6709−6717.
(54) Mourits, F. M.; Rummens, F. H. A. A critical evaluation of Lennard-Jones and Stockmayer potential parameters and of some correlation methods. *Can. J. Chem.* **1977**, *55*, 3007−3020.
(55) Tardy, D. C.; Rabinovitch, B. S. Collisional Energy Transfer. Thermal Unimolecular Systems in the Low-Pressure Region. *J. Chem. Phys.* **1966**, *45*, 3720−3730.
(56) Nguyen, T. N.; Trang, H. T. T.; Nguyen, N. T.; Pham, T. V. Computational study of the reaction of C_3H_3 with HNCO and the decomposition of C_4H_4NO radicals. *Int. J. Chem. Kinet.* **2022**, *54*, 447−460.
(57) Li, S. H.; Guo, J. J.; Li, R.; Wang, F.; Li, X. Y. Theoretical prediction of rate constants for hydrogen abstraction by OH, H, O, CH_3, and HO_2 radicals from toluene. *J. Phys. Chem. A* **2016**, *120*, 3424−3432.
(58) Alecu, I. M.; Truhlar, D. G. Computational Study of the Reactions of Methanol with the Hydroperoxyl and Methyl Radicals. 1. Accurate Thermochemistry and Barrier Heights. *J. Phys. Chem. A* **2011**, *115*, 2811−2829.
(59) Washida, N.; Bayes, K. D. The reaction of methyl radical with atomic and molecular oxygen. *Int. J. Chem. Kinet.* **1976**, *8*, 777−794.
(60) Basco, N.; James, D. G. L.; James, F. C. A quantitative study of alkyl radical reactions by kinetic spectroscopy. II. Combination of the methyl radical with the oxygen molecule. *Int. J. Chem. Kinet.* **1972**, *4*, 129−149.
(61) Hoare, D. E.; Walsh, A. D. The reaction of methyl radicals with oxygen and comparison with other third-order reactions. *Trans. Faraday Soc.* **1957**, *53*, 1102−1110.
(62) Avramenko, L. I.; Postnikov, L. M. The kinetics and mechanism of the interaction of methyl radicals with molecular oxygen. *Russ. Chem. Bull.* **1960**, *9*, 1796−1802.
(63) Ruscic, B.; Pinzon, R. E.; Laszewski, G. V.; Kodeboyina, D.; Burcat, A.; Leahy, D.; Montoya, D.; Wagner, A. F. Active Thermochemical Tables: thermochemistry for the 21st century. *J. Phys.: Conf. Ser.* **2005**, *16*, 561−570.
(64) Ruscic, B.; Pinzon, R. E.; Morton, M. L.; Srinivasan, N. K.; Su, M. C.; Sutherland, J. W.; Michael, J. V. Active Thermochemical Tables: Accurate Enthalpy of Formation of Hydroperoxyl Radical, HO_2. *J. Phys. Chem. A* **2006**, *110*, 6592−6601.

https://doi.org/10.1021/acsomega.3c01029
ACS Omega 2023, 8, 17005−17016